ACS APPLIED MATERIALS & INTERFACES

Research Article

Cite This: ACS Appl. Mater. Interfaces 2019, 11, 18494−18503

www.acsami.org

Machine Learning the Voltage of Electrode Materials in Metal-Ion Batteries

Rajendra P. Joshi,[†,‡] Jesse Eickholt,[‡] Liling Li,[‡] Marco Fornari,[†] Veronica Barone,*[,†] and Juan E. Peralta[†]

[†]Department of Physics and Science of Advanced Materials Program and [‡]Department of Computer Science, Central Michigan University, Mount Pleasant, Michigan 48859, United States

Supporting Information

ABSTRACT: Machine-learning (ML) techniques have rapidly found applications in many domains of materials chemistry and physics where large data sets are available. Aiming to accelerate the discovery of materials for battery applications, in this work, we develop a tool (http://se.cmich.edu/batteries) based on ML models to predict voltages of electrode materials for metal-ion batteries. To this end, we use deep neural network, support vector machine, and kernel ridge regression as ML algorithms in combination with data taken from the Materials Project database, as well as feature vectors from properties of chemical compounds and elemental properties of their constituents. We show that our ML models have predictive capabilities for different reference test sets and, as an example, we utilize them to generate a voltage profile diagram and compare it to density functional theory calculations. In addition, using our models, we propose nearly 5000 candidate electrode materials for Na- and K-ion batteries. We also make available a web-accessible tool that, within a minute, can be used to estimate the voltage of any bulk electrode material for a number of metal ions. These results show that ML is a promising alternative for computationally demanding calculations as a first screening tool of novel materials for battery applications.

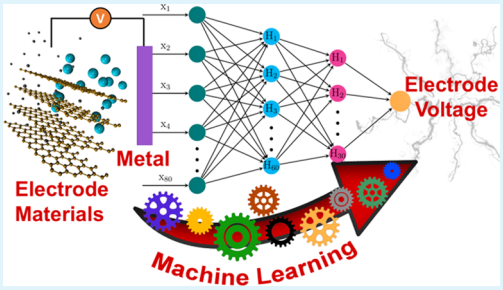

KEYWORDS: *machine learning, batteries, intercalation electrodes, web tool, voltage predictor, voltage profile diagram*

INTRODUCTION

Lithium-ion batteries (LIBs) have revolutionized the energy storage technology[1,2] and played a crucial role in transforming portable devices in terms of performance, lifetime, weight, and size. They have also opened unprecedented possibilities for new greener technologies, for instance, in the automotive sector.[2,3] Despite currently being the dominating energy source for small energy-scale devices, the transferability of traditional LIBs to higher energy scales remains a challenge mainly because of their relatively low energy density.[4−7] Moreover, the future of large-scale applications of LIBs is uncertain due to the scarcity of Li as raw material, its increasing price, skyrocketing energy demand, and safety concerns.[8−10] These issues call for more sustainable, cheaper, and better-performing alternatives to the present technology.

Several new designs for metal-ion batteries have been proposed in the literature, including monovalent Na- and K-ion batteries and multivalent Mg-, Ca-, and Al-ion batteries.[3−5,11−13] The development of these batteries has been limited mainly because of a lack of suitable electrode and electrolyte materials, stimulating considerable work devoted to enhancing their robustness.[14] For electrode materials, the number of possible compounds that could intercalate metal ions such as Li, Na, K, Mg, Ca, and Al is likely in the order of thousands; however, the majority of these materials remain unexplored as electrode components because of the experimental and computational difficulties to screen the large chemical and structural spaces with appropriate accuracy.[15−17] In this context, data-driven machine-learning (ML) approaches provide ways to address this issue faster and with limited use of computational resources.[18,19]

ML-based search for new electrode materials requires a sufficient amount of well-curated and verified data.[20] Recently, enabled by the significant improvement in computing architectures, several databases based on density functional theory (DFT) calculations such as AFLOW,[21,22] Materials Project,[23,24] OQMD,[25,26] and NOMAD[27] were made readily available to the scientific community. Although DFT predictions are not the gold standard for theoretical calculations in some contexts,[28] they do provide reasonable insights and can be used to guide experimental research.[29] In several cases, these electronic structure databases have been combined with ML approaches for predicting specific properties of interest in target materials.[16,22,30−34] For example, Seko et al.[35,36] used the kernel ridge regression (KRR) and support vector regression (SVR) to predict the cohesive energy of binary and ternary compounds, thermal conductivity of binary inorganic compounds, and melting temperature of single- and

Received: March 20, 2019
Accepted: April 29, 2019
Published: April 29, 2019

DOI: 10.1021/acsami.9b04933
ACS Appl. Mater. Interfaces 2019, 11, 18494−18503

binary-component solids. Similarly, Meredig et al.[37] built an ML model to predict the thermodynamic stability of any arbitrary chemical composition and proposed nearly 4500 new stable chemical compounds. ML approaches have also been used to improve the quality of exchange−correlation functionals in DFT.[38−40] These approaches have also been applied for the prediction of the band gap, total energy, and to find the potential candidate materials for photovoltaic cells, glass alloys, etc.[41−43] Logistic regression was used by Sendek et al.[44] to screen nearly 12 000 solids containing Li to propose new materials for electrolytes in Li-ion batteries. Similarly, online tools for ML predictions of electronic, thermal, and mechanical properties have been made available lately.[22]

In this work, we employ ML to develop a tool to predict electrode voltages for metal-ion batteries, using data from the Materials Project database. One of the challenges associated with an ML approach in material science is the problem of finding the proper feature vectors that can accurately represent the compounds.[45−47] In the literature, feature vectors derived from several approaches have been used.[46−49] A simple, yet effective, approach is the one derived from chemical, structural, elemental, and electronic representation of the compounds.[46] Here, we utilize the feature vectors derived from the chemical properties of compounds and the properties of their elemental constituents in combination with deep neural networks (DNNs),[50,51] support vector machine (SVM),[52] and kernel ridge regression (KRR).[53] Voltage profile diagrams generated from ML methods are compared to the corresponding DFT-based diagrams. We also provide a web-accessible interface that predicts the voltage of any electrode material (for any metal-ion battery) with minimal basic information and within minutes. Our work shows that ML models can be employed as an exploratory tool to predict the voltage of electrode materials very efficiently.

Our training data were extracted from the Material Project database containing a total of 4250 data instances for 3580 intercalation-based electrode materials.[23,24] We utilized the Material Project's application programming interface pymatgen to access the data from the database.[23,24] Each data instance corresponds to the average voltage calculated for material in between two concentrations of the intercalating metal ion. For some electrodes, average voltages are calculated for multiple concentrations, resulting in more data instances in comparison to the number of electrode materials. A total of 3977 data instances were kept after removing inconsistencies and repetitions. The data set that we use contains DFT-predicted voltages for several metal-ion batteries such as Li, Mg, Ca, Al, Zn, and Y. Nearly 65% of the data corresponds to Li-ion battery materials, while data for Ca-, Mg-, and Zn-ion batteries comprise 10% each in the database. Additionally, 4% of data instances correspond to Y- and Al-ion batteries. The database provides the average voltage of materials starting from completely deintercalated to fully intercalated (e.g., $C_6 \rightarrow LiC_6$, considering C_6 as the electrode material and Li as the metal), as well as from partially intercalated to fully intercalated (e.g., $Li_{0.5}C_6 \rightarrow LiC_6$).

The features used to specify a particular electrode material in our ML models include the working ion in the battery (i.e., Li or other metals), the concentration of the active metal ion in a given compound, crystal lattice types, and space group numbers. All other features were obtained from the elemental properties of the atomic constituents involved in a particular electrode. The elemental properties added to the feature vectors are adopted from the work of Ward et al.[41] and are listed in the Supporting Information (SI). This results in 237 features that uniquely represent each compound in the data set. The components of a feature vector are diverse in terms of their magnitudes, which can range from a few thousands to small fractions. Therefore, all of the input features were normalized for better and more efficient training of the model that avoids any biased preference of a particular feature with respect to others based solely on their magnitude. Normalization was performed by effectively scaling all of the inputs to be between −1 and 1, and it was carried out on the fly while training our model and it is not done for target values.

To systematically remove the redundancy within the feature vectors and also to reduce the dimensionality of the feature space, we used principal component (PC) analysis[54,55] algorithms, as implemented in the sklearn library.[56] In Figure 1, we show the cumulative explained variance as a function of the number of principal components (PCs). It shows that only 80 PCs are required, reducing the dimension of feature space significantly. Thus, only these 80 PCs were fed into our ML models.

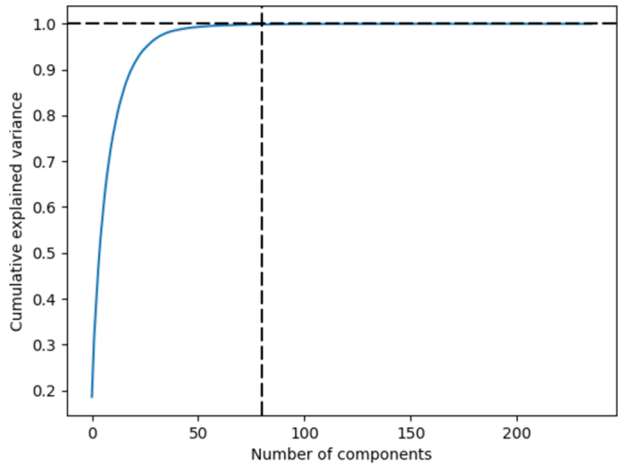

Figure 1. Principal component analysis for the feature vectors leads to a reduction of 66% of the dimensionality.

Our data were split into two parts, the training set (T-set, 90%) and the holdout test set (H-set, 10%). The T-set is randomly shuffled and used for parameter optimization with 10-fold cross-validation. In the 10-fold cross-validation, data are randomly divided into 10 equal segments (known as folds), and data in 9 of these folds are used for training the models and the remaining fold for validating the model. This is repeated 10 times in a way that each of the folds is used as the validation set. Independent validation of the models was done with the H-set, which is not utilized during the training process. In addition, we also examined the performance of our models on a limited Na-ion battery data set (Na-set) taken from the literature.[57] To assess the performance of our machine-learning models, we utilize the mean absolute error (MAE) defined as

$$\mathrm{MAE} = \frac{1}{N}\sum_{i}^{N} |Y^{i}_{\mathrm{target}} - Y^{i}_{\mathrm{predicted}}| \quad (1)$$

where Y^{i}_{target} and $Y^{i}_{\mathrm{predicted}}$ are the target and predicted values using our models for a given set of parameters for each material i, and N is the number of instances in the data set.

DOI: 10.1021/acsami.9b04933
ACS Appl. Mater. Interfaces 2019, 11, 18494−18503

RESULTS AND DISCUSSION

With the goal of assessing the performance of different ML algorithms, we have employed three machine-learning algorithms: DNN, SVM, and KRR. This assessment allows us to select the most robust model for our web tool. A four-layer DNN was used in our work with an architecture shown in Figure 2. To limit overfitting, we added a dropout layer[58] after

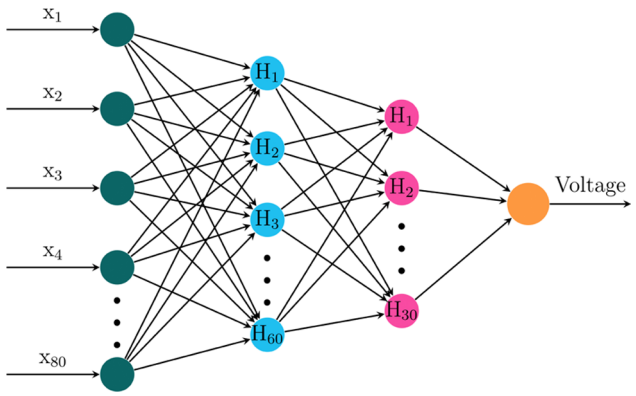

Figure 2. Architecture of the deep neural network used in our work. x_i are the inputs for the input layer and H_i represents nodes in hidden layers. The output from the output layer is the voltage.

the second and third layers with rates of 25 and 10%, respectively. In addition, we used the L2 regularization technique in our work.[59] In the input layer, we have 80 nodes with 60 and 30 nodes in the first and second hidden layers, respectively, and one node in the output layer. All of these parameters were tuned for the optimal performance of the model in the T-set and were chosen optimal when we obtained minimum MAE and when we did not detect signs of overfitting and underfitting. We have used mean-square error as loss function and MAE as a metric to measure the performance of the model, as implemented in the Keras machine-learning library.[60] We used "rmsprop" as an algorithm to optimize the loss function.

The MAE and the standard deviation for each fold in the T-set (computed with the optimal parameters) are shown in Table 1. We obtained similar MAE in all 10-folds of the DNN model with a mean MAE of 0.43 V and a standard deviation of ±0.03 V. We obtained a similar MAE of 0.43 V in the H-set. The performance of the model in the H-set is shown in Figure 4a, where a linear relationship between the target and DNN-predicted values is clearly shown.

We compared the performance of DNN with another machine-learning model, SVM. When used for a regression problem, SVM is known as a support vector regression (SVR). SVR is a kernel-based regression technique known for its robust performance in complex data representations. It works by mapping nonlinearly separable data in real space to higher dimensional space via a kernel function. We have used the radial basis function (RBF) kernel for this work. In addition, SVR depends on two important parameters (C and γ) that control the quality of the result. These parameters were tuned by using the grid search algorithm of sklearn. We varied C and γ logarithmically in between each 10^{-5} and 10^{5}. For each of the possible combinations of C and γ, SVR computations were performed using 10-fold cross-validation to calculate the mean of the MAE. The parameter space and MAE encoded as color, obtained from a grid search, are shown in Figure 3a. We determined the optimal values of C and γ such that they yield the minimum MAE from the grid search, which corresponds to an optimal combination of C = 10.0 and γ = 0.1, for which we obtain a mean MAE of 0.42 ± 0.13 V in the T-set. Further refining the grid in the small range around the optimal values of C and γ does not qualitatively influence our results. The MAEs for each fold of the 10-fold cross-validated T-set obtained with these tuned parameters and the RBF kernel are given in Table 1. The performance of SVR for the H-set is shown in Figure 4b.

In addition to SVR, the performance of DNN was compared with another kernel-based ML algorithm known as kernel ridge regression (KRR). Similarly to SVR, we used a grid search technique to find the optimal parameters α and γ by varying each between 10^{-5} and 10^{5}, which is shown in Figure 3b. In this case, we obtained optimal values of α and γ as 0.01 and 0.1, respectively, for which KRR yields a mean MAE of 0.46 ± 0.14 V in the T-set. The MAEs in the 10-folds of the T-set for the KRR model are given in Table 1 alongside the values obtained from DNN and SVR. Finally, we checked the performance on the H-set, which is shown in Figure 4c. We

Table 1. Mean Absolute Error (V) for Each Fold of 10-Fold Cross-Validation Using Deep Neural Network (DNN), Support Vector Regression (SVR), and Kernel Ridge Regression (KRR)[a]

fold	DNN	SVR	KRR
1	0.42	0.51	0.54
2	0.48	0.25	0.28
3	0.42	0.26	0.27
4	0.44	0.35	0.47
5	0.44	0.38	0.43
6	0.42	0.62	0.71
7	0.43	0.43	0.42
8	0.41	0.59	0.62
9	0.45	0.53	0.57
10	0.48	0.28	0.30
mean MAE ± standard deviation	0.43 ± 0.03	0.42 ± 0.13	0.46 ± 0.14
MAE H-set	0.43	0.40	0.39
MAE Na-set	1.25	1.00	0.93

[a]The mean and the standard deviation of the MAE in these 10 cross-validation sets are given. In addition, the MAEs for the H-set and Na-set are provided.

DOI: 10.1021/acsami.9b04933
ACS Appl. Mater. Interfaces 2019, 11, 18494−18503

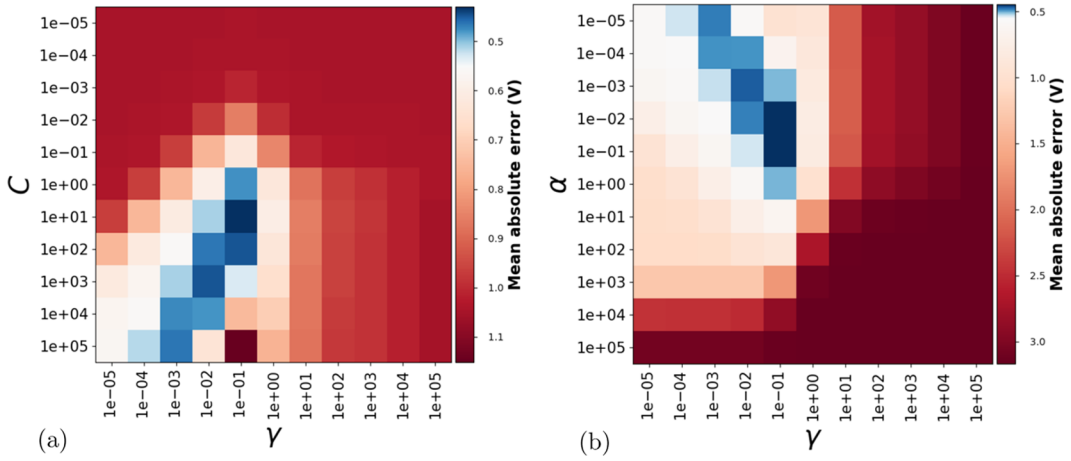

Figure 3. Color maps showing the tuning of (a) C and γ parameters for support vector regression and (b) α and γ parameters for kernel ridge regression. The color bars display the mean absolute error.

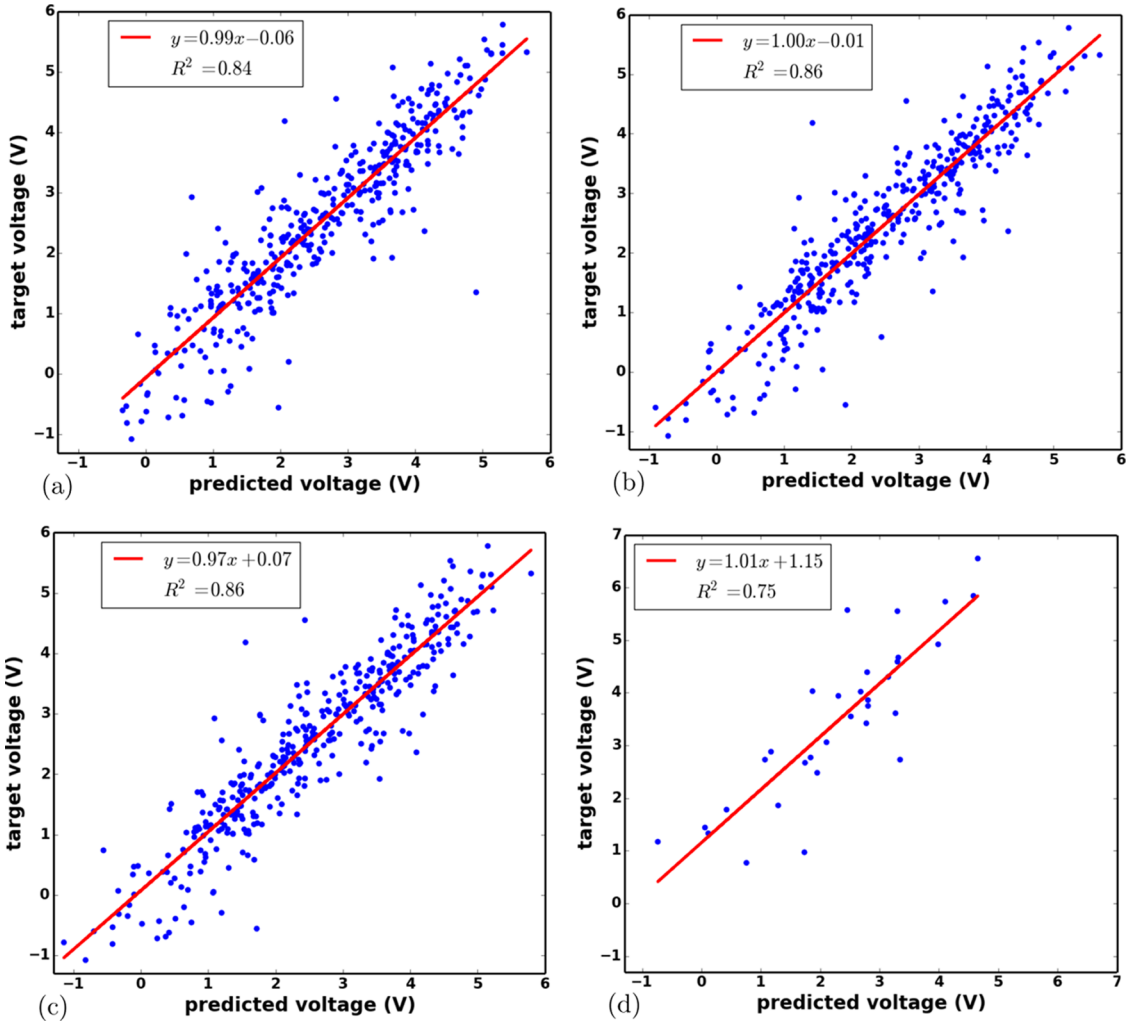

Figure 4. Scatter plot showing target vs predicted voltages with different ML algorithms used in this work. (a) DNN, (b) SVR, and (c) KRR, each on H-set. (d) DNN on Na-set. The best-fit equation ($y = mx + c$) and R^2 values for linear fit between target and ML-predicted values are provided as an inset.

obtained an MAE of 0.39 V on the H-set, which is in agreement with what we observed using SVR (0.40 V). These MAEs for the H-set depend only marginally on the ML algorithms, although, with SVR and KRR, there are minor deviations between the folds related to the kernel-based nature of both SVR and KRR: as we move between the folds, the data might not be that separable in folds when mapped using the kernel functions.

DOI: 10.1021/acsami.9b04933
ACS Appl. Mater. Interfaces 2019, 11, 18494−18503

Table 2. Mean Absolute Error (V) for Each Fold of 10-Fold Cross-Validated T-Set, H-Set, and Na-Set with DNN, SVR, and KRR along with Mean and Standard Deviation in MAE for the Models Trained on Li-Set[a]

fold	DNN	SVR	KRR
1	0.44	0.65	0.64
2	0.45	0.37	0.45
3	0.53	0.30	0.34
4	0.43	0.36	0.37
5	0.48	0.43	0.42
6	0.50	0.79	0.78
7	0.48	0.47	0.46
8	0.43	0.39	0.40
9	0.48	0.68	0.73
10	0.46	0.57	0.53
mean MAE ± standard deviation	0.47 ± 0.03	0.50 ± 0.15	0.51 ± 0.15
MAE H-set	0.42	0.44	0.44
MAE Na-set	0.70	0.62	0.70

[a]Note that the T-set and H-set here are taken from the Li-only data set.

The performance of our ML models on the H-set is shown in Figure 4a−c. We show in these scatter plots that for lower-voltage ranges the models perform slightly worse than for the higher-voltage range. We attribute this behavior to the limited amount of data available for training the model in this range. Such a limited amount of data might not be sufficient to capture the complexity of the patterns needed to predict voltages properly. We believe that the performance of the model in the low-voltage region could be improved by adding more data points within this range to the T-set.

For each model, we also show in Figure 4a−c the best-fit linear equation and the R^2 value as a measure of goodness of fit between the ML-predicted and the target values in the holdout test set. In the ideal case, the equation of best fit should be $y = x$, whereas R^2 should be one. With our models, we observed this relationship between the target and the ML-predicted values. In addition, the good performance of our models is also reflected in the R^2 values. We obtained reasonable R^2 values of 0.84, 0.86, and 0.86 with DNN, SVR, and KRR, respectively.

We note that although our ML models perform well and consistently, a more challenging test for the models would be achieved by gauging the performance of our models on a completely new data set. To this end, we checked the performance of the models on the Na-set. This data set is taken from the work of Zhang et al.[57] and contains voltage information of 32 Na-battery electrode materials with voltages in the range of 0.7−6.5 V. This set of materials was obtained by screening the entire Materials Project database for Na-based layered materials and then performing DFT calculations on the selected set of materials suitable as battery electrodes. The Na-set differs from the original T- and H-sets as it contains the voltage for Na-based electrode materials (for which our model is not trained). Thus, this is an excellent test to examine the robustness and the transferability of our ML models. In Table 1, we list the MAE obtained for the Na-set with each of the ML models. In addition, in Figure 4d, we show the scatter plots obtained with DNN. We observed that the model does not perform as well for Na-set as it does during cross-validation for the T- and H-sets. We obtained an MAE of about 0.8 V larger than in the case of the T- and H-sets using DNN. Despite the large MAE, the linear relationship between the predicted and target values is still preserved with our ML models. However, the poorer performance of the models for this test set is reflected in the relatively small R^2 value, as well as the best-fit line with large intercept. We identified two main reasons that could explain the comparatively poorer performance of our models in the Na-set. First, our model is not trained for Na-ion electrodes due to the lack of data in the databases for Na. Second, the Na-test set contains only 32 materials, which can affect the statistical performance of the ML models.

Li-Only Data. Our data set is diverse as it contains six different metal-ion (Li, Ca, Mg, Zn, Al, and Y) battery electrodes in a relatively small amount of data. It is interesting to see how the ML models perform on a specific metal-ion battery data. As a representative case, and due to the availability of a relatively large proportion of data for Li-ion electrodes, we trained our ML models only on Li-only battery data (Li-set). The model parameters are tuned again with Li-only data using the same protocol as we used for the entire data (parameters are provided in the SI). The MAE obtained from all three ML models in the 10-fold cross-validated T-set, H-set, and Na-set are given in Table 2. We note that the T-set and H-set used in this case are 90% and 10% of the Li-only data, respectively. The corresponding scatter plots in the H-set are provided in the SI.

Although the performance of the models in the T-set and H-set, as quantified by the MAE, is similar to the one obtained considering the entire data set, the performance on the Na-set is improved in comparison to the models trained on the entire data set (see Table 1). Such an improvement might be due to the more coherent data for training the models, as well as the similarity between Na-ion and Li-ion electrochemistry. In the case of models trained only on Li data, an MAE of 0.62−0.70 V is obtained for the Na-set with all three models, which is slightly larger than what we obtained for the other test sets. This larger error is somewhat expected, and still promising, considering that the model is not trained for Na-battery electrode materials and the small number statistics effect in the Na-set. Nonetheless, these results show that our ML models are transferable among different metal-ion batteries.

In Figure 5, we show the scatter plot obtained by using DNN on the Na-set. The performance of DNN on this new test set is similar to what we observed for the original Li-only training and test sets. The ML-predicted voltage values follow a linear trend with respect to the target voltage. The improved performance on Na-set can also be seen from the best-fit equation ($y = 1.11x + 0.17$, compared to the entire data best-fit equation $y = 1.01x + 1.15$ on Na-set). Additionally, we observe

DOI: 10.1021/acsami.9b04933
ACS Appl. Mater. Interfaces 2019, 11, 18494−18503

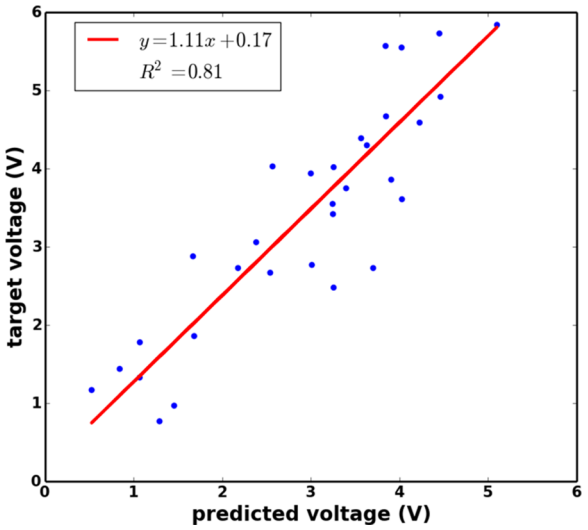

Figure 5. Scatter plot showing the target vs the predicted values (V) with DNN trained on the Li-set and applied to the Na-set, which is taken from the work of Zhang et al.[57] (other scatter plots are available in the SI).

an improvement in the R^2 value with the model trained only on Li data batteries for the Na-set. Similar results were obtained with SVR and KRR (the corresponding scatter plots are provided in the SI).

Voltage Profiles. The ML models we developed in this work can be used to generate the voltage profile diagram for electrode materials. These diagrams provide an estimate of the voltage range that an electrode can supply when used in a battery. To obtain these diagrams, one needs to evaluate voltages at different intercalation concentrations. Our ML method offers a fast alternative to DFT methods on estimating this voltage. As an example, in Figure 6, we show the voltage

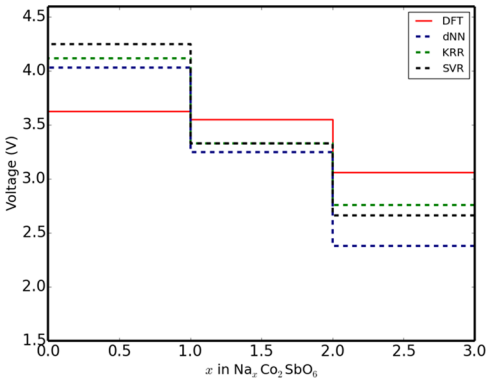

Figure 6. Voltage profile diagram obtained from different ML models and DFT for $Na_xCo_2SbO_6$. The DFT values are taken from the work of Zhang et al.[57]

profile diagram of the Na-based electrode material $Na_xCo_2SbO_6$, obtained from ML models, and compare it with the one obtained using DFT, as reported by Zhang et al.[57] In the voltage profile diagrams, we observe that as the concentration of Na-ion increases, the DFT voltage decreases gradually. The same pattern is observed with the DNN-predicted voltage in the electrode material considered. This trend is also reproduced by the other two machine-learning algorithms (SVR and KRR), as shown in Figure 6.

Application: Prediction of New Electrodes. The potential of our ML models to propose new electrode materials for Na- and K-ion batteries is assessed by studying candidate materials that are known for Li-ion but not necessarily explored for Na- and K-ion batteries. In the literature, some of the materials used as electrode for Li-ion have also been studied for their use as electrodes in Na-ion batteries. For instance, Ceder et al.[61] presented a comparative study for a set of selected cathode materials in terms of the voltage they offer when used as Li- and Na-ion battery electrodes. They found that a material provides on average 0.18−0.57 V lower voltage when used as an electrode for Na-ion battery than the corresponding Li-based electrodes, in agreement with experimental observations in some of these materials.

Although the generalization of their conclusion for all possible Li- and Na-based electrode materials is not documented, the trend observed from their study is encouraging, as it implies that electrode materials that have been known over the last two decades for their use in Li-ion batteries can potentially work as electrodes in Na- and K-ion batteries operating at lower voltages. The majority of Li-based electrode materials existing in the MP database are not explored for Na- and K-ion battery electrodes. A quantitative estimate of their performance for Na- and K-ion batteries is necessary to build a robust and cheaper alternative to Li-ion batteries. Here, we use our ML tool to examine the performance of Li-based electrode materials found in the MP database for Na and K by replacing the intercalating Li-ion with Na- and K-ions. We utilize the same stoichiometry and crystal structure for Na- and K-intercalated materials as in the parent Li-based material. The goal of this exercise is to propose new cathodes for Na- and K-ion batteries, predict their voltage, and study the correlation of predicted voltage with respect to that of Li-ion.

We first verify the conclusion of Ceder et al.[61] by taking a few materials from their work and calculating the voltage of these materials for Li-, Na-, and K-ions, using our DNN ML model. These results are shown in Table 3, where we include

Table 3. ML-Predicted Voltage (V) for Li-, Na-, and K-Based Electrodes[a]

material	A = Li	A = Na	A = K
$ACoO_2$	3.56 (3.99, 4.10)	3.40 (3.48, 2.80)	3.26
$ANiO_2$	3.81 (3.82, 3.85)	3.61 (3.31, 3.00)	3.12
$ATiO_2$	1.96 (1.94)	1.79 (1.37, >1.50)	1.51
$ATiS_2$	1.71 (1.82)	1.66 (1.64)	1.53
$AFePO_4$	3.36 (3.45, 3.50)	2.95 (3.08, 3.00)	2.39
$AMnPO_4$	3.66 (3.89, 4.10)	3.30 (3.59)	2.69
$ACoPO_4$	4.03 (4.64, 4.8)	3.53 (4.19)	2.85
$ANiPO_4$	4.50 (5.06, 5.3)	4.12 (4.58)	3.28
$A_3V_2(PO_4)_3$	3.54 (3.13, 3.8)	3.11 (2.94)	2.59

[a]Corresponding DFT and experimental values (when available) are provided in parentheses. DFT voltages, experimental references, and materials were taken from the work of Ceder et al.[61]

DFT and experimental values when available. Our ML model reproduced the trend observed from DFT calculations. ML-predicted voltages for Na-ion materials are on average 0.30 V smaller than the corresponding Li values. This is comparable to the 0.40 V shift observed from DFT calculations for the same materials. The voltages predicted for K-ion materials are even

DOI: 10.1021/acsami.9b04933
ACS Appl. Mater. Interfaces 2019, 11, 18494−18503

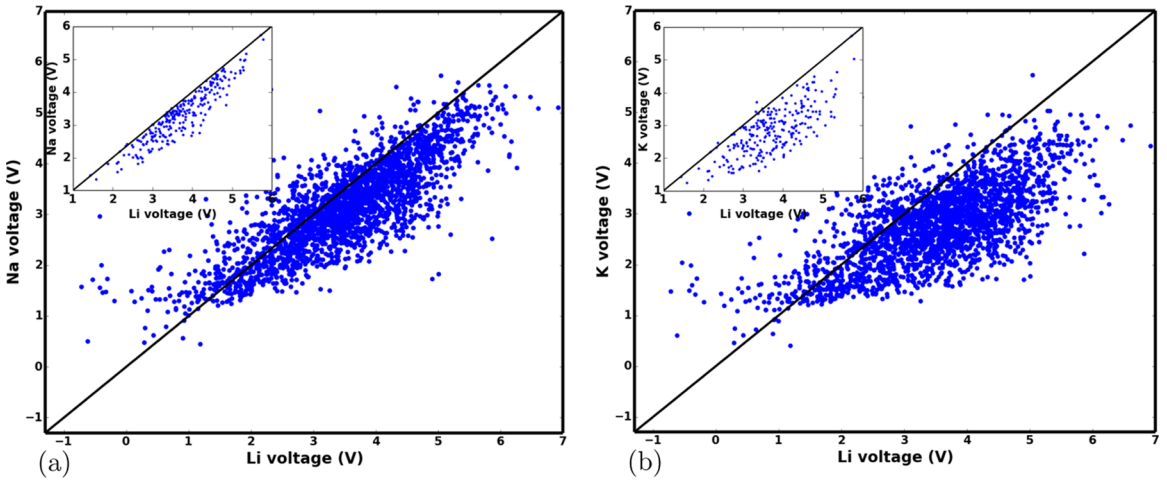

Figure 7. Scatter plots showing ML-predicted voltages for electrode materials obtained by replacing Li-ions with (a) Na-ions and (b) K-ions with respect to the corresponding DFT Li-voltages. The inset shows the ML-predicted voltages for Na- and K-ions in the H-set of Li-only materials with the corresponding ML-predicted voltages for Li-ion. The $y = x$ line is drawn as a reference for the eye.

Table 4. DNN-Predicted vs Experimental Average Voltage (V) for Different Electrodes

electrode	ML	experiment	electrode	ML	experiment
$NaMnO_2$	2.98	2.75[a]	$LiFePO_4$	3.36	3.50[b]
$NaCoO_2$	3.40	2.80[b]	$LiNiO_2$	3.81	3.85[b]
$NaTiO_2$	1.79	>1.50[b]	$NaFe_{0.5}Co_{0.5}O_2$	3.58	3.14[d]
$NaNiO_2$	3.61	3.00[b]	$K_{1.6}Na_2Mn_3O_7$	2.74	2.20[e]
$LiCoO_2$	3.60	4.10[b]	$Mg_2Mo_6S_8$	1.09	1.30[f]
$NaFePO_4$	2.95	3.00[b]	$Mg_{0.55}TiSe_2$	1.63	1.45[g]
$Na_4MnV(PO4)_3$	3.42	3.00[c]	$MgMoO_3$	2.20	2.25[h]

[a]Taken from ref 62. [b]Taken from ref 61. [c]Taken from ref 63. [d]Taken from ref 64. [e]Taken from ref 65. [f]Taken from ref 66. [g]Taken from ref 67. [h]Taken from ref 68.

smaller than the corresponding voltages in Na-ion materials. Overall, the average voltages follow the trend Li > Na > K.

The voltage of new electrode materials based on Na- and K-ions is shown in Figure 7a, where we show the scatter plot of the ML-predicted voltages of Na-based electrodes against the DFT-predicted voltage of Li-based electrodes for the same materials. For the majority of the materials studied, the conclusion of Ceder et al. remains valid: ML-predicted voltages for Na-based electrodes are, in general, smaller than the corresponding Li ones. We obtained a mean difference and mean absolute difference between DFT Li-voltages and ML-predicted Na-voltages of 0.36 and 0.56 V, respectively.

For several electrodes, however, a larger voltage is predicted by our model for Na-based electrodes compared to the corresponding Li-based DFT values. This overestimation might arise because we are comparing ML-predicted voltages of Na-ion against DFT voltages of Li-ion. A better comparison for such correlation, perhaps, should consider ML-predicted voltages for both ions. To this end, we compared the ML-predicted voltage for the H-set used in the Li-only case for both Li- and Na-ions. The resulting scatter plot is shown in the inset of Figure 7a. In this case, all of the predicted voltages for Na-electrodes are smaller than the corresponding ones for Li-electrodes. The corresponding scatter plots for DFT Li-voltage and ML-predicted voltage for Na- and K-based electrode materials in the H-set are provided in the SI (Figure S4). We obtained a mean deviation of 0.42 V in the H-set, which is consistent with the trend observed by Ceder et al.[61]

A similar analysis was performed for K-based electrodes. We observed that voltages calculated for K-ion are even smaller than in Na- and Li-ions. The corresponding scatter plot is given in Figure 7b. ML-predicted K-voltages are in general smaller by 0.73 V compared to DFT Li-voltages. With respect to Li-electrodes in the H-set, ML-predicted K-voltages are smaller on average by 0.91 V. The ML-predicted voltages for Na- and K-based electrodes are provided in the SI along with the DFT voltages for the corresponding Li-electrodes.

With this analysis, we have identified a vast number of materials as well as their corresponding voltages that could work as suitable electrodes for Na- and K-ion batteries. From this first screening, researchers could further refine a set of materials in terms of structures, maximum metal stoichiometries, and voltages using DFT methods and, ultimately, experiments.

Web Tool for Voltage Prediction. We implemented a publicly available web-accessible tool for the battery community that can be used to predict the voltage of any novel electrode with minimal basic information typically within a minute. The only information required to predict the voltage are the stoichiometry of the intercalated material at high ion concentration, the stoichiometry of the material at low ion concentration, the type of metal-ion battery, the fraction of metal ions corresponding to the stoichiometry of the material at high ion concentration, the crystal lattice type, and the space group. This information is readily available for any material with a crystalline structure, making our tool efficient as well as remarkably easy to use. We used our most robust model,

DOI: 10.1021/acsami.9b04933
ACS Appl. Mater. Interfaces 2019, 11, 18494−18503

DNN, as a back-end ML model in our online tool for voltage prediction. Our tool can be used to predict the average voltage of Li-, Na-, K-, Mg-, Ca-, Zn-, Al-, and Y-ion battery electrodes. Li-only trained model is used for the prediction of voltage for battery electrodes based on Li-, Na-, and K-ions, whereas the entire data set trained model is used for the rest of ions. This tool can be freely accessed at http://se.cmich.edu/batteries.

Knowing the performance of the web tool in comparison to experimental reference might be of interest to the community exploring the electrode material experimentally. As proof of concept, we compare the predicted average voltages with experimental average voltages. We selected a few electrode materials from the literature[61−63,65−70] and calculated their average voltage using the web tool. These results are summarized in Table 4, where we observe a good agreement between the predicted voltages and the corresponding experimental values.

CONCLUSIONS

In conclusion, we used deep neural network, support vector regression, and kernel ridge regression to machine learn the voltage of electrode materials in a given metal-ion battery, utilizing DFT data extracted from the Materials Project database. The performance of the models is gauged by comparing the mean absolute error between the training set, the holdout test set, and data from the literature. Our results indicate that ML models reproduce DFT trends and thus can be used to explore electrode materials in terms of voltages. This methodology is fast compared to DFT calculations and can be used to guide experiments seeking to develop novel materials for battery applications or to perform a quick screening before starting synthesis procedures. Using our models, we propose nearly 5000 electrode materials for Na- and K-ion batteries. Further improvement in the performance of the model might be necessary for the routine application of ML algorithms for the prediction of the voltage of electrode materials. Such improvements might include, but are not limited to, using other machine-learning algorithms, using more data, or exploring other ways of feeding intercalation reactions to the ML models. In addition, for the robust training of ML models in the future, DFT calculation records of electrode materials in all voltage ranges should be kept in the databases (even if a material is not suitable as a battery electrode) since negative data instances are also required for proper training of data-intensive models. We also provide a web-accessible tool that can be used to predict the voltage of any electrode material within a minute.

ASSOCIATED CONTENT

Supporting Information

The Supporting Information is available free of charge on the ACS Publications website at DOI: 10.1021/acsami.9b04933.

Scatter plots showing the performance of several ML models on the holdout test sets and the Na-test set; color map showing the parameter tuning in Li-only data; a table with the voltages predicted by DNN, SVM, and KRR for Na-set along with the DFT values; and a table with the ML-predicted voltage of Na- and K-based electrodes along with the DFT values for Li-based electrodes (PDF)

AUTHOR INFORMATION

Corresponding Author

*E-mail: v.barone@cmich.edu.

ORCID

Juan E. Peralta: 0000-0003-2849-8472

Notes

The authors declare no competing financial interest.

ACKNOWLEDGMENTS

The authors acknowledge the Material Project database for the data used in this work. R.P.J. thanks Dr Kai Trepte for careful proofreading of the manuscript. R.P.J. also thanks Dr Zhen Zhou and Dr Xu Zhang for providing the DFT intercalation voltage for the voltage profile diagram. This work was supported by the Office of Basic Energy Sciences, US Department of Energy, DE-SC0005027 and DE-SC0019432.

REFERENCES

(1) Winter, M.; Barnett, B.; Xu, K. Before Li Ion Batteries. *Chem. Rev.* **2018**, *118*, 11433−11456.

(2) Nitta, N.; Wu, F.; Lee, J. T.; Yushin, G. Li-ion Battery Materials. *Mater. Today* **2015**, *18*, 252−264.

(3) Eames, C.; Islam, M. S. Ion Intercalation into Two-Dimensional Transition-Metal Carbides: Global Screening for New High-Capacity Battery Materials. *J. Am. Chem. Soc.* **2014**, *136*, 16270−16276.

(4) Joshi, R. P.; Ozdemir, B.; Barone, V.; Peralta, J. E. Hexagonal BC_3: A Robust Electrode Material for Li, Na, and K Ion Batteries. *J. Phys. Chem. Lett.* **2015**, *6*, 2728−2732.

(5) Bhauriyal, P.; Mahata, A.; Pathak, B. Hexagonal BC_3 Electrode for a High-Voltage Al-Ion Battery. *J. Phys. Chem. C* **2017**, *121*, 9748−9756.

(6) Posada, J. O. G.; Rennie, A. J.; Villar, S. P.; Martins, V. L.; Marinaccio, J.; Barnes, A.; Glover, C. F.; Worsley, D. A.; Hall, P. J. Aqueous Batteries as Grid Scale Energy Storage Solutions. *Renewable Sustainable Energy Rev.* **2017**, *68*, 1174−1182.

(7) Dunn, B.; Kamath, H.; Tarascon, J.-M. Electrical Energy Storage for the Grid: a Battery of Choices. *Science* **2011**, *334*, 928−935.

(8) Liu, K.; Liu, Y.; Lin, D.; Pei, A.; Cui, Y. Materials for Lithium-Ion Battery Safety. *Sci. Adv.* **2018**, *4*, No. eaas9820.

(9) Tarascon, J.-M.; Armand, M. *Materials For Sustainable Energy: A Collection of Peer-Reviewed Research and Review Articles from Nature Publishing Group*; World Scientific, 2011; pp 171−179.

(10) Tarascon, J.-M. Is Lithium the New Gold? *Nat. Chem.* **2010**, *2*, 510.

(11) Guduru, R. K.; Icaza, J. C. A Brief Review on Multivalent Intercalation Batteries with Aqueous Electrolytes. *Nanomaterials* **2016**, *6*, 41.

(12) Kulish, V. V.; Koch, D.; Manzhos, S. Ab initio Study of Li, Mg and Al Insertion into Rutile VO_2: Fast Diffusion and Enhanced Voltages for Multivalent Batteries. *Phys. Chem. Chem. Phys.* **2017**, *19*, 22538−22545.

(13) Thackeray, M. M.; Wolverton, C.; Isaacs, E. D. Electrical Energy Storage for Transportation-Approaching the Limits of, and going Beyond, Lithium-Ion Batteries. *Energy Environ. Sci.* **2012**, *5*, 7854−7863.

(14) Rajput, N. N.; Seguin, T. J.; Wood, B. M.; Qu, X.; Persson, K. A. *Modeling Electrochemical Energy Storage at the Atomic Scale*; Korth, M., Ed.; Springer International Publishing: Cham, 2018; pp 79−124.

(15) Kirkpatrick, P.; Ellis, C. Chemical Space. *Nature* **2004**, *432*, 823.

(16) von Lilienfeld, O. A. Quantum Machine Learning in Chemical Compound Space. *Angew. Chem., Int. Ed.* **2018**, *57*, 4164−4169.

(17) Mullard, A. The Drug-maker's Guide to the Galaxy. *Nature* **2017**, *549*, 445.

(18) Ghahramani, Z. Probabilistic Machine Learning and Artificial Intelligence. *Nature* **2015**, *521*, 452.

(19) Jordan, M. I.; Mitchell, T. M. Machine Learning: Trends, Perspectives, and Prospects. *Science* **2015**, *349*, 255−260.
(20) Fornari, M.; Marzari, N. The 2019 materials by design roadmap. *J. Phys. D: Appl. Phys.* **2018**, *52*, No. 013001, DOI: 10.1088/1361-6463/aad926.
(21) Curtarolo, S.; Setyawan, W.; Hart, G. L.; Jahnatek, M.; Chepulskii, R. V.; Taylor, R. H.; Wang, S.; Xue, J.; Yang, K.; Levy, O.; Mehl, M. J.; Stokes, H. T.; Demchenko, D. O.; Morgan, D. AFLOW: An Automatic Framework for High-Throughput Materials Discovery. *Comput. Mater. Sci.* **2012**, *58*, 218−226.
(22) Gossett, E.; Toher, C.; Oses, C.; Isayev, O.; Legrain, F.; Rose, F.; Zurek, E.; Carrete, J.; Mingo, N.; Tropsha, A.; Curtarolo, S. AFLOW-ML: A RESTful API for machine-learning predictions of materials properties. *Comput. Mater. Sci.* **2018**, *152*, 134−145.
(23) Jain, A.; Ong, S. P.; Hautier, G.; Chen, W.; Richards, W. D.; Dacek, S.; Cholia, S.; Gunter, D.; Skinner, D.; Ceder, G.; Persson, K. A. Commentary: The Materials Project: A Materials Genome Approach to Accelerating Materials Innovation. *APL Mater.* **2013**, *1*, No. 011002.
(24) Ong, S. P.; Cholia, S.; Jain, A.; Brafman, M.; Gunter, D.; Ceder, G.; Persson, K. A. The Materials Application Programming Interface (API): A Simple, Flexible and Efficient API for Materials Data based on REpresentational State Transfer (REST) principles. *Comput. Mater. Sci.* **2015**, *97*, 209−215.
(25) Saal, J. E.; Kirklin, S.; Aykol, M.; Meredig, B.; Wolverton, C. Materials Design and Discovery with High-Throughput Density Functional Theory: The Open Quantum Materials Database (OQMD). *JOM* **2013**, *65*, 1501−1509.
(26) Kirklin, S.; Saal, J. E.; Meredig, B.; Thompson, A.; Doak, J. W.; Aykol, M.; Rühl, S.; Wolverton, C. The Open Quantum Materials Database (OQMD): Assessing the Accuracy of DFT Formation Energies. *npj Comput. Mater.* **2015**, *1*, No. 15010.
(27) Draxl, C.; Scheffler, M. NOMAD: The FAIR concept for big data-driven materials science. *MRS Bull.* **2018**, *43*, 676−682.
(28) Joshi, R. P.; Trepte, K.; Withanage, K. P. K.; Sharkas, K.; Yamamoto, Y.; Basurto, L.; Zope, R. R.; Baruah, T.; Jackson, K. A.; Peralta, J. E. Fermi-Löwdin Orbital Self-Interaction Correction to Magnetic Exchange Couplings. *J. Chem. Phys.* **2018**, *149*, No. 164101.
(29) Kaloni, T. P.; Joshi, R. P.; Adhikari, N. P.; Schwingenschlögl, U. Band Gap Tunning in BN-doped Graphene Systems with High Carrier Mobility. *Appl. Phys. Lett.* **2014**, *104*, No. 073116.
(30) Ramprasad, R.; Batra, R.; Pilania, G.; Mannodi-Kanakkithodi, A.; Kim, C. Machine Learning in Materials Informatics: Recent Applications and Prospects. *npj Comput. Mater.* **2017**, *3*, 54.
(31) Bassman, L.; Rajak, P.; Kalia, R. K.; Nakano, A.; Sha, F.; Sun, J.; Singh, D. J.; Aykol, M.; Huck, P.; Persson, K.; Vashishta, P. Active Learning for Accelerated Design of Layered Materials. *npj Comput. Mater.* **2018**, *4*, 74.
(32) Zhang, Y.; Ling, C. A Strategy to Apply Machine Learning to Small Datasets in Materials Science. *npj Comput. Mater.* **2018**, *4*, 25.
(33) Butler, K. T.; Davies, D. W.; Cartwright, H.; Isayev, O.; Walsh, A. Machine Learning for Molecular and Materials Science. *Nature* **2018**, *559*, 547.
(34) Schleder, G. R.; Padilha, A. C. M.; Acosta, C. M.; Costa, M.; Fazzio, A. From DFT to Machine Learning: Recent Approaches to Materials Science - A Review. *J. Phys. Mater.* **2019**, 11−12.
(35) Seko, A.; Hayashi, H.; Nakayama, K.; Takahashi, A.; Tanaka, I. Representation of Compounds for Machine-Learning Prediction of Physical Properties. *Phys. Rev. B* **2017**, *95*, No. 144110.
(36) Seko, A.; Maekawa, T.; Tsuda, K.; Tanaka, I. Machine Learning with Systematic Density-Functional Theory Calculations: Application to Melting Temperatures of Single- and Binary-Component Solids. *Phys. Rev. B* **2014**, *89*, No. 054303.
(37) Meredig, B.; Agrawal, A.; Kirklin, S.; Saal, J. E.; Doak, J. W.; Thompson, A.; Zhang, K.; Choudhary, A.; Wolverton, C. Combinatorial Screening for New Materials in Unconstrained Composition Space with Machine Learning. *Phys. Rev. B* **2014**, *89*, No. 094104.
(38) Brockherde, F.; Vogt, L.; Li, L.; Tuckerman, M. E.; Burke, K.; Müller, K.-R. Bypassing the Kohn-Sham equations with machine learning. *Nat. Commun.* **2017**, *8*, No. 872.
(39) Mills, K.; Spanner, M.; Tamblyn, I. Deep Learning and the Schrödinger Equation. *Phys. Rev. A* **2017**, *96*, No. 042113.
(40) Li, L.; Snyder, J. C.; Pelaschier, I. M.; Huang, J.; Niranjan, U.-N.; Duncan, P.; Rupp, M.; Müller, K.-R.; Burke, K. Understanding Machine-Learned Density Functionals. *Int. J. Quantum Chem.* **2016**, *116*, 819−833.
(41) Ward, L.; Agrawal, A.; Choudhary, A.; Wolverton, C. A General-Purpose Machine Learning Framework for Predicting Properties of Inorganic Materials. *npj Comput. Mater.* **2016**, *2*, No. 16028.
(42) Faber, F. A.; Lindmaa, A.; von Lilienfeld, O. A.; Armiento, R. Machine Learning Energies of 2 Million Elpasolite (ABC_2D_6) Crystals. *Phys. Rev. Lett.* **2016**, *117*, No. 135502.
(43) Deml, A. M.; O'Hayre, R.; Wolverton, C.; Stevanović, V. Predicting Density Functional Theory Total Energies and Enthalpies of Formation of Metal-nonmetal Compounds by Linear Regression. *Phys. Rev. B* **2016**, *93*, No. 085142.
(44) Sendek, A. D.; Yang, Q.; Cubuk, E. D.; Duerloo, K.-A. N.; Cui, Y.; Reed, E. J. Holistic Computational Structure Screening of more than 12,000 Candidates for Solid Lithium-ion Conductor Materials. *Energy Environ. Sci.* **2017**, *10*, 306−320.
(45) Isayev, O.; Oses, C.; Toher, C.; Gossett, E.; Curtarolo, S.; Tropsha, A. Universal Fragment Descriptors for Predicting Properties of Inorganic Crystals. *Nat. Commun.* **2017**, *8*, No. 15679.
(46) Ghiringhelli, L. M.; Vybiral, J.; Levchenko, S. V.; Draxl, C.; Scheffler, M. Big Data of Materials Science: Critical Role of the Descriptor. *Phys. Rev. Lett.* **2015**, *114*, No. 105503.
(47) Rupp, M.; von Lilienfeld, O. A.; Burke, K. Guest Editorial: Special Topic on Data-Enabled Theoretical Chemistry. *J. Chem. Phys.* **2018**, *148*, No. 241401.
(48) Hansen, K.; Biegler, F.; Ramakrishnan, R.; Pronobis, W.; von Lilienfeld, O. A.; Müller, K.-R.; Tkatchenko, A. Machine Learning Predictions of Molecular Properties: Accurate Many-Body Potentials and Nonlocality in Chemical Space. *J. Phys. Chem. Lett.* **2015**, *6*, 2326−2331.
(49) Ward, L.; Liu, R.; Krishna, A.; Hegde, V. I.; Agrawal, A.; Choudhary, A.; Wolverton, C. Including Crystal Structure Attributes in Machine Learning Models of Formation Energies via Voronoi Tessellations. *Phys. Rev. B* **2017**, *96*, No. 024104.
(50) LeCun, Y.; Bengio, Y.; Hinton, G. Deep Learning. *Nature* **2015**, *521*, 436−444.
(51) Goodfellow, I.; Bengio, Y.; Courville, A.; Bengio, Y. *Deep Learning*; MIT Press Cambridge, 2016; Vol. *1*.
(52) Noble, W. S. What is a Support Vector Machine? *Nat. Biotechnol.* **2006**, *24*, 1565−1567.
(53) Vovk, V. In *Kernel Ridge Regression*; Schoelkopf, B. et al., Ed.; Springer, 2013; pp 105−116.
(54) Pearson, K. LIII. On Lines and Planes of Closest Fit to Systems of Points in Space. *London, Edinburgh Dublin Philos. Mag. J. Sci.* **1901**, *2*, 559−572.
(55) Jolliffe, I. *International Encyclopedia of Statistical Science*; Springer, 2011; pp 1094−1096.
(56) Pedregosa, F.; Varoquaux, G.; Gramfort, A.; Grisel, O.; Michel, V.; Thirion, B.; Blondel, M.; Prettenhofer, P.; Weiss, R.; Dubourg, V.; Vanderplas, J.; Passos, A.; Cournapeau, D.; Brucher, M.; Perrot, M.; Duchesnay, E. Scikit-learn: Machine Learning in Python. *J. Mach. Learn. Res.* **2011**, *12*, 2825−2830.
(57) Zhang, X.; Zhang, Z.; Yao, S.; Chen, A.; Zhao, X.; Zhou, Z. An Effective Method to Screen Sodium-based Layered Materials for Sodium Ion Batteries. *npj Comput. Mater.* **2018**, *4*, 13.
(58) Srivastava, N.; Hinton, G.; Krizhevsky, A.; Sutskever, I.; Salakhutdinov, R. Dropout: A Simple Way to Prevent Neural Networks from Overfitting. *J. Mach. Learn. Res.* **2014**, *15*, 1929−1958.
(59) Ng, A. Y. In *Feature Selection, L1 vs L2 Regularization, and Rotational Invariance*, Proceedings of the Twenty-First International Conference on Machine Learning, 2004; p 78.

DOI: 10.1021/acsami.9b04933
ACS Appl. Mater. Interfaces 2019, 11, 18494−18503

(60) Chollet, F. Keras: Deep Learning Library for Theano and Tensorflow, 2015. https://keras.io.
(61) Ong, S. P.; Chevrier, V. L.; Hautier, G.; Jain, A.; Moore, C.; Kim, S.; Ma, X.; Ceder, G. Voltage, stability and diffusion barrier differences between sodium-ion and lithium-ion intercalation materials. *Energy Environ. Sci.* **2011**, *4*, 3680−3688.
(62) Billaud, J.; Clément, R. J.; Armstrong, A. R.; Canales-Vázquez, J.; Rozier, P.; Grey, C. P.; Bruce, P. G. β-$NaMnO_2$: A High-Performance Cathode for Sodium-Ion Batteries. *J. Am. Chem. Soc.* **2014**, *136*, 17243−17248.
(63) Nisar, U.; Shakoor, R.; Essehli, R.; Amin, R.; Orayech, B.; Ahmad, Z.; Kumar, P. R.; Kahraman, R.; Al-Qaradawi, S.; Soliman, A. Sodium Intercalation/de-intercalation Mechanism in $Na_4MnV(PO_4)_3$ Cathode materials. *Electrochim. Acta* **2018**, *292*, 98−106.
(64) Yoshida, H.; Yabuuchi, N.; Komaba, S. $NaFe_{0.5}Co_{0.5}O_2$ as High Energy and Power Positive Electrode for Na-ion Batteries. *Electrochem. Commun.* **2013**, *34*, 60−63.
(65) Sada, K.; Senthilkumar, B.; Barpanda, P. Potassium-Ion Intercalation Mechanism in Layered $Na_2Mn_3O_7$. *ACS Appl Energy Mater.* **2018**, *1*, 5410−5416.
(66) Canepa, P.; Sai Gautam, G.; Hannah, D. C.; Malik, R.; Liu, M.; Gallagher, K. G.; Persson, K. A.; Ceder, G. Odyssey of Multivalent Cathode Materials: Open Questions and Future Challenges. *Chem. Rev.* **2017**, *117*, 4287−4341.
(67) Gu, Y.; Katsura, Y.; Yoshino, T.; Takagi, H.; Taniguchi, K. Rechargeable Magnesium-ion Battery based on a $TiSe_2$-Cathode with d-p orbital Hybridized Electronic Structure. *Sci. Rep.* **2015**, *5*, No. 12486.
(68) Gershinsky, G.; Yoo, H. D.; Gofer, Y.; Aurbach, D. Electrochemical and Spectroscopic Analysis of Mg^{2+} Intercalation into Thin Film Electrodes of Layered Oxides: V_2O_5 and MoO_3. *Langmuir* **2013**, *29*, 10964−10972.
(69) Recham, N.; Rousse, G.; Sougrati, M. T.; Chotard, J.-N.; Frayret, C.; Mariyappan, S.; Melot, B. C.; Jumas, J.-C.; Tarascon, J.-M. Preparation and Characterization of a Stable $FeSO_4F$-Based Framework for Alkali Ion Insertion Electrodes. *Chem. Mater.* **2012**, *24*, 4363−4370.
(70) Wang, L.; Zou, J.; Chen, S.; Zhou, G.; Bai, J.; Gao, P.; Wang, Y.; Yu, X.; Li, J.; Hu, Y.-S.; Li, H. TiS_2 as a High Performance Potassium Ion Battery Cathode in Ether-based Electrolyte. *Energy Storage Mater.* **2018**, *12*, 216−222.

DOI: 10.1021/acsami.9b04933
ACS Appl. Mater. Interfaces 2019, 11, 18494−18503